

Inelastic processes in strontium–hydrogen collisions and their impact on non-LTE calculations

Svetlana A. Yakovleva,^{1*} Andrey K. Belyaev,¹ Lyudmila I. Mashonkina,²

¹*Department of Theoretical Physics and Astronomy, Herzen University, St. Petersburg 191186, Russia*

²*Institute of Astronomy of the Russian Academy of Sciences, Pyatnitskaya st. 48, 119017, Moscow, Russia*

Accepted XXX. Received YYY; in original form ZZZ

ABSTRACT

Inelastic processes rate coefficients for low-energy Sr + H, Sr⁺ + H⁻, Sr⁺ + H and Sr²⁺ + H⁻ collisions are calculated using multichannel quantum model approach. 31 scattering channels of SrH⁺ and 17 scattering channels of SrH are considered. The partial cross sections and the partial rate coefficients are hence calculated for 1202 partial processes in total. Using new quantum data for Sr II + H I collisions, we updated model atom of Sr II and performed the non-local thermodynamic equilibrium (non-LTE) calculations. We provide the non-LTE abundance corrections for the Sr II resonance lines in two grids of model atmospheres, which are applicable to very metal-poor ([Fe/H] ≤ -2) dwarfs and giants.

Key words: atomic collisional data; atomic inelastic processes; rate coefficients; stars: atmospheres

1 INTRODUCTION

The stars with a mass of less than the solar one have a long lifetime comparable with the Galaxy age, and they play an important role in providing observational material for the Galactic chemical evolution studies. One of the directions of such studies is a restoration of the synthesis history for heavy nuclei produced by the neutron-capture nuclear reactions. In these reactions, neutrons are captured by nuclei that can then undergo β decay if they are unstable, transforming neutrons into protons and producing elements of the higher atomic number. Depending on the neutron flux available which determines the lifetime for neutron capture, τ_n , the neutron-capture mechanisms are separated into the slow (s-) processes and the rapid (r-) processes (Burbidge et al. 1957). If τ_n is greater than the radioactive decay lifetime, τ_β , for unstable nuclei, the process is referred to as a slow (s-) process, and the process is defined as a rapid (r-) process, if $\tau_n \ll \tau_\beta$. Different isotopes have different yields from the neutron-capture nuclear reactions, either s- or r-process, with relatively sharp peaks at the magic numbers $N_n = 50$ and 82 on the abundance curve, N_n being a number of neutrons. Strontium (Sr) is the best observed of the elements beyond the Fe group. The most abundant isotopes of strontium, ⁸⁸Sr, ⁸⁷Sr, and ⁸⁶Sr, have $N_n = 50$, 49 , and 48 ; thus, strontium is related to the first peak. The best representative of the second peak elements is barium (Ba). In the solar system matter, abundances of both Sr and Ba are mostly contributed from the main s-process occurring during thermally pulsing asymptotic giant branch (AGB) phase of low mass ($1.3 \leq M/M_\odot < 4$) stars, with fractions of s-nuclei of about 70 and 85 %, respectively (Bisterzo et al. 2014). In the early Universe, before the onset of the

main s-process, the r-process is expected to be the only source of the neutron-capture elements. Observations of barium and the heavier elements in very metal-poor (VMP, [Fe/H] ≤ -2), old stars provide evidence for their r-process origin (Snedden et al. 2008). The origin of the first peak elements and strontium among them is less clear.

If Ba and Sr were produced by the same nucleosynthesis source and before the onset of the main s-process, this would result in a fairly flat [Sr/Ba] ratio versus [Ba/H] for VMP stars. This is not supported by the observations. For the Galactic halo stars, McWilliam et al. (1995); Honda et al. (2004), and François et al. (2007) find increasing [Sr/Ba] ratio towards lower [Ba/H]. Similar tight anti-correlation of [Sr/Ba] with [Ba/H] is found by Mashonkina et al. (2017) for the VMP stars in not only our Galaxy, but also its satellites – classical dwarf spheroidal galaxies (dSphs). The latter paper reports also on the second group of stars, which reveal similar [Sr/Ba] ~ -0.5, in line with the empirical r-process ratio, [Sr/Ba]_r = -0.44 ± 0.08 (Barklem et al. 2005). Thus, observations of VMP stars suggest that, in the early Universe, there existed the second nucleosynthesis channel for Sr, besides the classical r-process.

The extra source(s) of Sr is (are) not identified yet despite various ideas and nucleosynthesis models which have been proposed in the literature, see the most recent paper by Rizzuti et al. (2019) and references therein. Further progress can be provided by improving observational constraints to the theoretical models. Therefore, one needs to improve an accuracy of the derived stellar abundances of Sr and Ba, as well as to increase their statistics. In order to determine accurate elemental abundances, the theoretical spectra should be calculated based on the non-local thermodynamic equilibrium (non-LTE = NLTE) line formation. For barium, the non-LTE modelings using on the most up-to-date methods and atomic data

* E-mail: sayakovleva@herzen.spb.ru

available so far, including the quantum rate coefficients calculated by [Belyaev & Yakovleva \(2018\)](#) for the inelastic processes in Ba I, Ba II + H I and Ba II, Ba III + H⁻ collisions, were already treated ([Mashonkina & Belyaev 2019](#); [Gallagher et al. 2020](#)). The present paper is devoted to strontium.

In VMP stars, strontium is observed in lines of Sr II. The non-LTE methods for Sr II were developed by [Belyakova & Mashonkina \(1997\)](#); [Andrievsky et al. \(2011\)](#), and [Bergemann et al. \(2012\)](#). They all treat the H I impact excitation and de-excitation processes using the [Steenbock & Holweger \(1984\)](#) formulas, which are based on the work of [Drawin \(1969\)](#). Such an approach has been criticized for not providing a realistic description of the physics involved and overestimating the collision rates ([Barklem et al. 2011](#)). This paper presents new quantum calculations of the Sr I + H I, Sr II + H I, Sr II + H⁻, and Sr III + H⁻ collisions. The obtained rate coefficients for the excitation and charge exchange processes by hydrogen impact were implemented in the model atom of Sr II. The model atom from [Belyakova & Mashonkina \(1997\)](#) was taken as a basic model.

In the following, Sect. 2 gives the description of the atomic data calculations. Two quasimolecules are considered: Ionic SrH⁺ and neutral SrH ones. The former collisional system is treated in the $J - J$ representation, that is, it includes the fine structure is taken into account, while the later in the $L - S$ representation, that is, without accounting for the fine structure. The brief description of the way to treat a nonadiabatic nuclear dynamics is presented. The results of the quantum calculations for the inelastic processes of neutralisation, ion-pair formation, excitations and de-excitation are discussed as well. Sect. 3 describes the updated model atom of Sr II and presents the non-LTE abundance corrections for the Sr II 4077, 4215 Å resonance lines in the two grids of model atmospheres, which are applicable to VMP dwarfs and giants. Sect. 4 concludes the article.

2 ATOMIC DATA CALCULATIONS

2.1 Processes in Sr⁺ + H and Sr²⁺ + H⁻ collisions

The electronic structure of a SrH⁺ quasimolecule was studied with *ab initio* methods by [Aymar & Dulieu \(2012\)](#) and more thoroughly by [Mejrissi et al. \(2018\)](#), although none of these studies was performed in a relativistic approximation and has any information about fine structure levels of a SrH⁺ quasimolecule.

In order to study inelastic processes in collisions of Sr⁺ with hydrogen atoms taking fine structure levels of Sr⁺ into account, nonadiabatic nuclear dynamics should be investigated in the JJ representation. The ionic molecular state Sr²⁺ ($4p^6 \ ^1S_0$) + H⁻ ($1s^2 \ ^1S_0$) has the same structure as in case of alkali-hydrogen collisions: both partners have closed electronic shells and the ionic molecular state has the 0⁺ symmetry. For such collisions an approach for taking fine structure of alkali-atoms into account in quantum model calculations was proposed in ([Belyaev et al. 2019](#)). This model suggests to use the asymptotic approach for calculations of diabatic potentials for A^{Z+} (1S_0) + H⁻ (1S_0) and A^{(Z-)+} (2L_j) + H ($^2S_{1/2}$) states. The off-diagonal diabatic Hamiltonian matrix elements for the fine struc-

ture levels are calculated dividing semiempirical matrix elements ([Olson et al. 1971](#)) proportional to the coefficients:

$$C = \frac{1}{\sqrt{2}} \left(\begin{bmatrix} j & 1/2 & J \\ 1/2 & -1/2 & 0 \end{bmatrix} \begin{bmatrix} L & 1/2 & j \\ 0 & 1/2 & 1/2 \end{bmatrix} - \begin{bmatrix} j & 1/2 & J \\ -1/2 & 1/2 & 0 \end{bmatrix} \begin{bmatrix} L & 1/2 & j \\ 0 & -1/2 & -1/2 \end{bmatrix} \right), \quad (1)$$

where the square brackets denote the Clebsch-Gordan coefficients.

This approach for electronic structure modelling allows one to take into account nonadiabatic transitions due to the interaction of the ionic and covalent configurations of a quasimolecule ([Belyaev 2013](#)). For this reason only covalent states of the 0⁺ molecular symmetry are taken into account. The calculations of the SrH⁺ electronic structure are performed for 31 scattering channels listed in Table 1: 30 covalent molecular states and one ionic. The non-adiabatic nuclear dynamics is investigated using the multichannel Landau-Zener approach described in detail in ([Belyaev et al. 2014](#); [Yakovleva et al. 2016](#)), the cross sections and rate coefficients are calculated for all inelastic processes due to transitions between these states.

In a multichannel case, a state-to-state probability for a transition from an initial channel i to a final channel f for the neutralization and de-excitation processes ($i > f$) is calculated by the following equations

$$P_{if}^{neutr} = 2p_f (1 - p_f) \left(\prod_{k=f+1}^{i-1} p_k \right) \left\{ 1 + \sum_{m=1}^{2(f-1)} \prod_{k=1}^m (-p_{f-[k/2]}) \right\},$$

$$P_{if}^{deex} = 2p_f (1 - p_f) (1 - p_i) \left(\prod_{k=f+1}^{i-1} p_k \right) \left\{ 1 + \sum_{m=1}^{2(f-1)} \prod_{k=1}^m (-p_{f-[k/2]}) \right\}, \quad (2)$$

where the nonadiabatic transition probability p_j after a single passing of a nonadiabatic region is calculated by means of the two-state Landau-Zener model ([Landau 1932a,b](#); [Zener 1932](#)) by the following formula

$$p_j = \exp \left(-\frac{\xi_j}{v} \right), \quad (3)$$

the Landau-Zener parameter ξ_j being computed by means of the adiabatic-potential based formula derived by [Belyaev & Lebedev \(2011\)](#)

$$\xi_j = \frac{\pi}{2\hbar} \sqrt{\frac{Z_j^3}{Z_j''}} \Big|_{R=R_C}. \quad (4)$$

In this equation, Z_j is the absolute value of the adiabatic potential splitting between neighbouring states: $Z_j(R) = |U_j(R) - U_{j\pm 1}(R)|$, R_C being a centre of a nonadiabatic region, R'' denotes the second derivative with respect to the internuclear distance R . The latter formula allows one to calculate the nonadiabatic transition probability only from the information about the adiabatic potentials without making transformation into a diabatic representation which is not uniquely defined and time-consuming. The partial cross sections and the partial rate coefficients are calculated from the state-to-state transition probabilities as usual, see, e.g., Ref. ([Belyaev 2013](#)).

Let us discuss the results of the rate coefficients calculations. The graphical representation of the calculated rate coefficients for the temperature $T = 6000$ K is shown in Figure 1, where rate

Table 1. SrH⁺ (k 0⁺) molecular states (in the *JJ* representation), the corresponding scattering channels, their asymptotic energies with respect to the ground-state level (taken from NIST, [Kramida et al. 2021](#)).

k	Scattering channels	Asymptotic energies (eV)
1	Sr ⁺ (4p ⁶ 5s ² S _{1/2}) + H(1s ² S _{1/2})	0.0
2	Sr ⁺ (4p ⁶ 4d ² D _{3/2}) + H(1s ² S _{1/2})	1.8047016
3	Sr ⁺ (4p ⁶ 4d ² D _{5/2}) + H(1s ² S _{1/2})	1.8394593
4	Sr ⁺ (4p ⁶ 5p ² P _{1/2} ^o) + H(1s ² S _{1/2})	2.9403088
5	Sr ⁺ (4p ⁶ 5p ² P _{3/2} ^o) + H(1s ² S _{1/2})	3.0396772
6	Sr ⁺ (4p ⁶ 6s ² S _{1/2}) + H(1s ² S _{1/2})	5.9185754
7	Sr ⁺ (4p ⁶ 5d ² D _{3/2}) + H(1s ² S _{1/2})	6.6066604
8	Sr ⁺ (4p ⁶ 5d ² D _{5/2}) + H(1s ² S _{1/2})	6.6174048
9	Sr ⁺ (4p ⁶ 6p ² P _{1/2} ^o) + H(1s ² S _{1/2})	6.91456
10	Sr ⁺ (4p ⁶ 6p ² P _{3/2} ^o) + H(1s ² S _{1/2})	6.95029
11	Sr ⁺ (4p ⁶ 4f ² F _{7/2} ^o) + H(1s ² S _{1/2})	7.561801
12	Sr ⁺ (4p ⁶ 4f ² F _{5/2} ^o) + H(1s ² S _{1/2})	7.561962
13	Sr ⁺ (4p ⁶ 7s ² S _{1/2}) + H(1s ² S _{1/2})	8.0545218
14	Sr ⁺ (4p ⁶ 6d ² D _{3/2}) + H(1s ² S _{1/2})	8.3717688
15	Sr ⁺ (4p ⁶ 6d ² D _{5/2}) + H(1s ² S _{1/2})	8.3767629
16	Sr ⁺ (4p ⁶ 7p ² P _{1/2} ^o) + H(1s ² S _{1/2})	8.515153
17	Sr ⁺ (4p ⁶ 7p ² P _{3/2} ^o) + H(1s ² S _{1/2})	8.532235
18	Sr ⁺ (4p ⁶ 5f ² F _{5/2} ^o) + H(1s ² S _{1/2})	8.811036
19	Sr ⁺ (4p ⁶ 5f ² F _{7/2} ^o) + H(1s ² S _{1/2})	8.811036
20	Sr ⁺ (4p ⁶ 5g ² G _{7/2}) + H(1s ² S _{1/2})	8.847240
21	Sr ⁺ (4p ⁶ 5g ² G _{9/2}) + H(1s ² S _{1/2})	8.847240
22	Sr ⁺ (4p ⁶ 8s ² S _{1/2}) + H(1s ² S _{1/2})	9.080243
23	Sr ⁺ (4p ⁶ 7d ² D _{3/2}) + H(1s ² S _{1/2})	9.251862
24	Sr ⁺ (4p ⁶ 7d ² D _{5/2}) + H(1s ² S _{1/2})	9.254565
25	Sr ⁺ (4p ⁶ 8p ² P _{3/2} ^o) + H(1s ² S _{1/2})	9.337473
26	Sr ⁺ (4p ⁶ 6f ² F _{7/2} ^o) + H(1s ² S _{1/2})	9.491412
27	Sr ⁺ (4p ⁶ 6f ² F _{5/2} ^o) + H(1s ² S _{1/2})	9.491412
28	Sr ⁺ (4p ⁶ 6g ² G _{7/2}) + H(1s ² S _{1/2})	9.514262
29	Sr ⁺ (4p ⁶ 6g ² G _{9/2}) + H(1s ² S _{1/2})	9.514262

Table 1 – continued – SrH⁺ (k 0⁺) molecular states (in the *JJ* representation), the corresponding scattering channels, their asymptotic energies with respect to the ground-state level (taken from NIST, [Kramida et al. 2021](#)).

k	Scattering channels	Asymptotic energies (eV)
30	Sr ⁺ (4p ⁶ 9s ² S _{1/2}) + H(1s ² S _{1/2})	9.653112
31	Sr ²⁺ (4p ⁶ 1S ₀) + H ⁻ (1s ² 1S ₀)	10.2762764

Table 2. SrH (k ²Σ⁺) molecular states, the corresponding scattering channels, their asymptotic energies with respect to the ground-state level (taken from NIST ([Kramida et al. 2021](#))).

k	Scattering channels	Asymptotic energies (eV)
1	Sr (5s ² 1S) + H(1s ² S)	0.0
2	Sr (5s5p ³ P ^o) + H(1s ² S)	1.8228877
3	Sr (5s4d ³ D) + H(1s ² S)	2.2631734
4	Sr (5s4d ¹ D) + H(1s ² S)	2.4982425
5	Sr (5s5p ¹ P ^o) + H(1s ² S)	2.6902652
6	Sr (5s6s ³ S) + H(1s ² S)	3.600349
7	Sr (5s6s ¹ S) + H(1s ² S)	3.7929029
8	Sr (4d5p ³ F ^o) + H(1s ² S)	4.1725763
9	Sr (4d5p ¹ D ^o) + H(1s ² S)	4.1940009
10	Sr (5s6p ³ P ^o) + H(1s ² S)	4.2061469
11	Sr (5s6p ¹ P ^o) + H(1s ² S)	4.2276633
12	Sr (5s5d ¹ D) + H(1s ² S)	4.3056546
13	Sr (5s5d ³ D) + H(1s ² S)	4.3431318
14	Sr (5p ² 3P) + H(1s ² S)	4.4051164
15	Sr (4d5p ³ D ^o) + H(1s ² S)	4.5181299
16	Sr (5s7s ³ S) + H(1s ² S)	4.6400683
17	Sr ⁺ (5s ² S) + H ⁻ (1s ² 1S)	4.9408674

coefficients are presented by color from blue to red according to the legend. One can see from Figure 1 that the rate coefficients with the highest values ($\geq 10^{-8}$ cm³/s) correspond to the neutralization processes to the following final states of a strontium ion: Sr⁺ (4p⁶6s²S_{1/2}), Sr⁺ (4p⁶5d²D_{3/2,5/2}), Sr⁺ (4p⁶6p²P_{1/2,3/2}), Sr⁺ (4p⁶4f²F_{7/2,5/2}) and Sr⁺ (4p⁶7s²S_{1/2}) (the scattering channels k = 6 – 13 in Table 1). At T = 6000 K, the rate coefficients have the values from 1.36×10^{-8} to 3.48×10^{-8} cm³/s. Several processes have rate coefficients with moderate values (from 10^{-10} to 10^{-8} cm³/s): mainly these are other neutralization processes and excitation / de-excitation processes associated with transitions between states k = 6 – 13 from Table 1.

Figure 2 shows the dependence of the neutralization rate coefficient

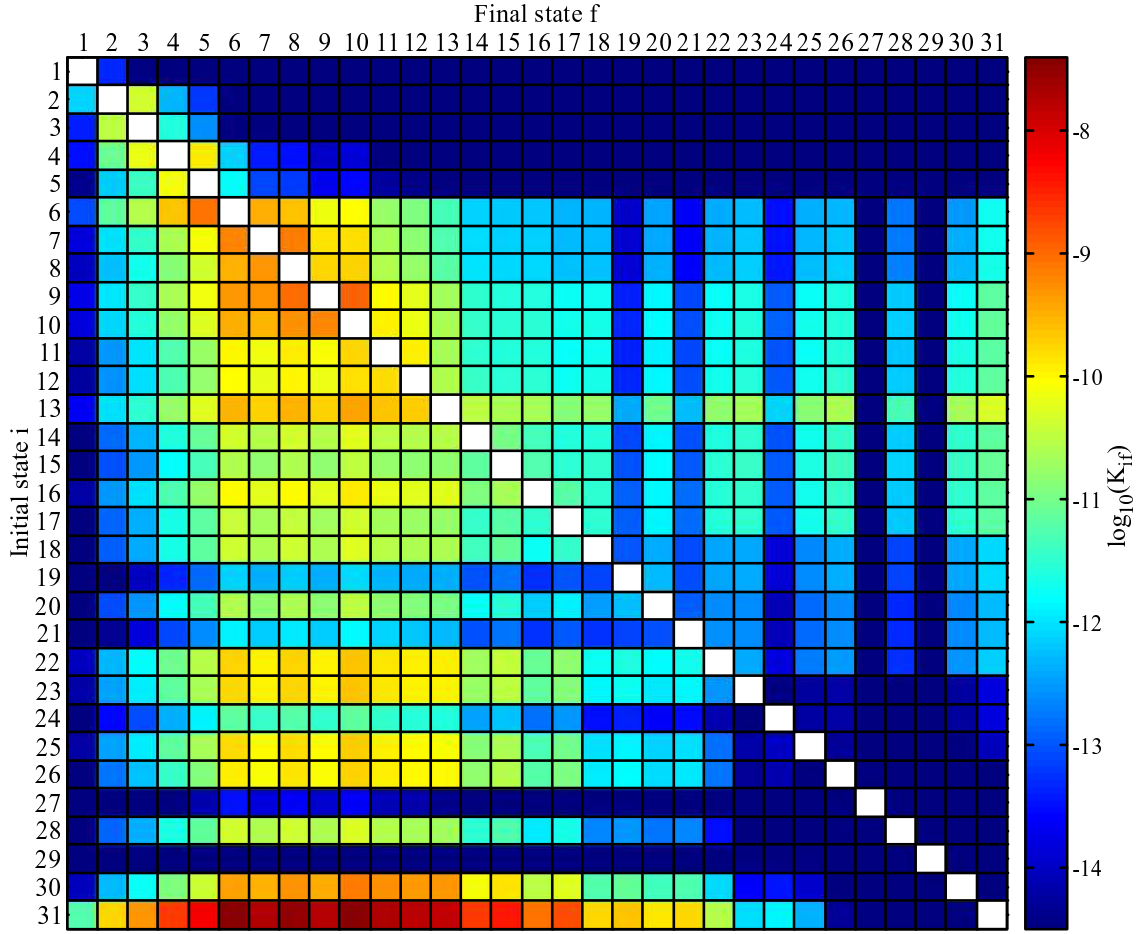


Figure 1. The graphical representation for the inelastic processes rate coefficients in $\text{Sr}^+ (4p^6nl^2L_j) + \text{H}(1s^2S_{1/2})$ and $\text{Sr}^{2+} (4p^6^1S_0) + \text{H}^-(1s^2^1S_0)$ collisions at the temperature $T = 6000$ K. The labels for the initial and final states are given in Table 1.

coefficients on the excitation energy of the final state calculated both with and without account for the fine structure levels of Sr^+ . The LS and JJ calculations give almost the same rate coefficients for neutralization processes to $\text{Sr}^+ (4p^6ns^2S_{1/2}) + \text{H}$ states that have only one fine structure level, while the results for the neutralization processes to other states show non-trivial behavior. Rate coefficients for the processes to fine structure levels can not be obtained by dividing the results of LS-calculations proportionally to the statistical populations of the final states or even proportionally to the coefficients given by Eq. (1). This is due to the reason that each nonadiabatic region is changed differently with the transition of the L-S representation to the J-J representation. This fact has different effects on the transition probabilities and eventually on the rate coefficients.

2.2 Processes in $\text{Sr} + \text{H}$ and $\text{Sr}^+ + \text{H}^-$ collisions

Calculations of rate coefficients for the inelastic processes in collisions of Sr atoms with hydrogen atoms are performed in L-S representation, that is without account for the fine structure levels of Sr. Same as for the case of SrH^+ we applied the asymptotic approach for SrH electronic structure modelling (Belyaev 2013) and multi-channel analytical Landau-Zener formulae for non-adiabatic nuclear

dynamics (Belyaev et al. 2014; Yakovleva et al. 2016). Ionic molecular state $\text{Sr}^+ (5s^2S) + \text{H}^- (1s^2^1S)$ has $^2\Sigma^+$ molecular symmetry, for this reason the investigation is performed within this symmetry. 17 scattering channels that form $^2\Sigma^+$ molecular states are considered and collected in Table 2 together with their asymptotic energies taken from NIST database (Kramida et al. 2021). Cross sections and rate coefficients are calculated for all inelastic processes due to the transitions between the states in Table 2.

Figure 3 shows the graphical representation of the calculated rate coefficients in SrH collisions. Only three inelastic processes have rate coefficients higher than 10^{-8} cm^3/s : two mutual neutralization processes $\text{Sr}^+ (5s^2S) + \text{H}^- (1s^2^1S) \rightarrow \text{Sr} (5s6s^1,3S) + \text{H}(1s^2S)$ and one de-excitation process $\text{Sr} (5s6s^1S) + \text{H}(1s^2S) \rightarrow \text{Sr} (5s6s^3S) + \text{H}(1s^2S)$. At the temperature $T = 6000$ K the corresponding values of the rate coefficients are $(4.92, 5.39, 1.32) \times 10^{-8}$ cm^3/s .

The mutual neutralization rate coefficients at $T = 6000$ K are presented in Figure 4 as a function of the excitation energy of the final state. One can see from Figure 4 that rate coefficients of the processes due to the one-electron transitions are in good agree-

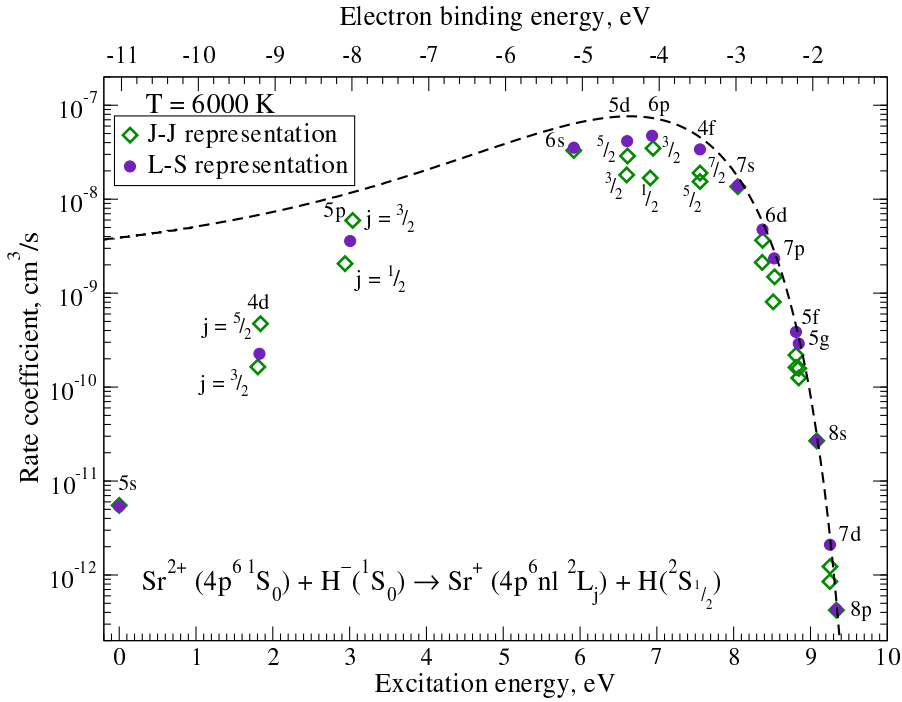


Figure 2. The rate coefficients (in cm^3/s) at $T = 6000 \text{ K}$ for the neutralization processes in $\text{Sr}^{2+}(4p^6 \ ^1S_0) + \text{H}^-(1s^2 \ ^1S_0)$ collisions. Empty diamonds correspond to the calculations with the account for the fine structure, filled circles – to the calculations without fine structure, dashed line shows the general dependence of the rate coefficient according to the simplified quantum model (Belyaev & Yakovleva 2017b).

ment with the general dependence of the rate coefficients given by the simplified quantum model (Belyaev & Yakovleva 2017a) which is plotted by the dashed line. The deviations from this behaviour at low excitation energies occur due to the presence of the long-range non-adiabatic regions. In this case the multichannel approach gives smaller values for the transition probabilities to the lower-lying states than the two-state approximation used in the simplified quantum model. This general dependence allows one to evaluate the optimal window for the energies of the scattering channels that are likely to be initial or final channels of the processes with high values of the rate coefficients. As for the processes due to the two-electron transitions they can not be considered with the simplified quantum model and are treated differently in electronic structure calculations. Non-adiabatic regions that correspond to two-electron transitions are usually very narrow even if the excitation energy of the covalent state lies in the optimal window, and that leads to small values of the transition probabilities in such regions.

3 NON-LTE CALCULATIONS FOR Sr II

3.1 Model atom of Sr II and method of calculations

We use a comprehensive model atom of Sr II that was constructed by Belyakova & Mashonkina (1997) and updated later by including electron-impact excitation rate coefficients from ab initio calculations of Bautista et al. (2002). In this study, we implemented the H I impact excitation and de-excitation processes in Sr II , with the rate coefficients described in Sect. 2.

We briefly describe the atomic data we used. The model atom includes 40 levels, up to 12d, of Sr II and the ground state of Sr III . The transition probabilities were taken from Reader et al. (1980);

Lindgård & Nielson (1977), and R. Kurucz website¹. Photoionization cross-sections for ns , np and nd levels have been calculated by the quantum defect method using Peach (1967) tables. For the remaining levels, we applied the hydrogenic approximation, where a principal quantum number n was replaced with an effective principal quantum number n_{eff} . We note that, for effective temperatures of $T_{\text{eff}} > 4000 \text{ K}$, Sr II is the majority species in the line formation layers, and the uncertainty in the adopted photoionization cross-sections affects only weakly the statistical equilibrium (SE) of Sr II . Bautista et al. (2002) provide accurate electron-impact excitation rate coefficients for all the transitions between 5s and up to 4f. The formula of van Regemorter (1962) for allowed transitions and the effective collision strength $Y = 1$ for forbidden transitions were used in the other cases. Ionization by electronic collisions was calculated from the Seaton (1962) formula, employing a hydrogenic photoionization cross-section at the threshold. The H I impact excitation and de-excitation processes were taken into account for all the transitions between 5s and up to 9s, using accurate rate coefficients from quantum calculations (Sect. 2).

To solve the coupled radiative transfer and SE equations, we employed the DETAIL code (Butler & Giddings 1985), where the opacity package was modified, as described by Mashonkina et al. (2011). The calculations were performed with the MARCS plane-parallel (1D) model atmospheres with standard abundances (Gustafsson et al. 2008) available on the MARCS web site².

¹ <http://kurucz.harvard.edu/atoms/3801/>

² <http://marcs.astro.uu.se>

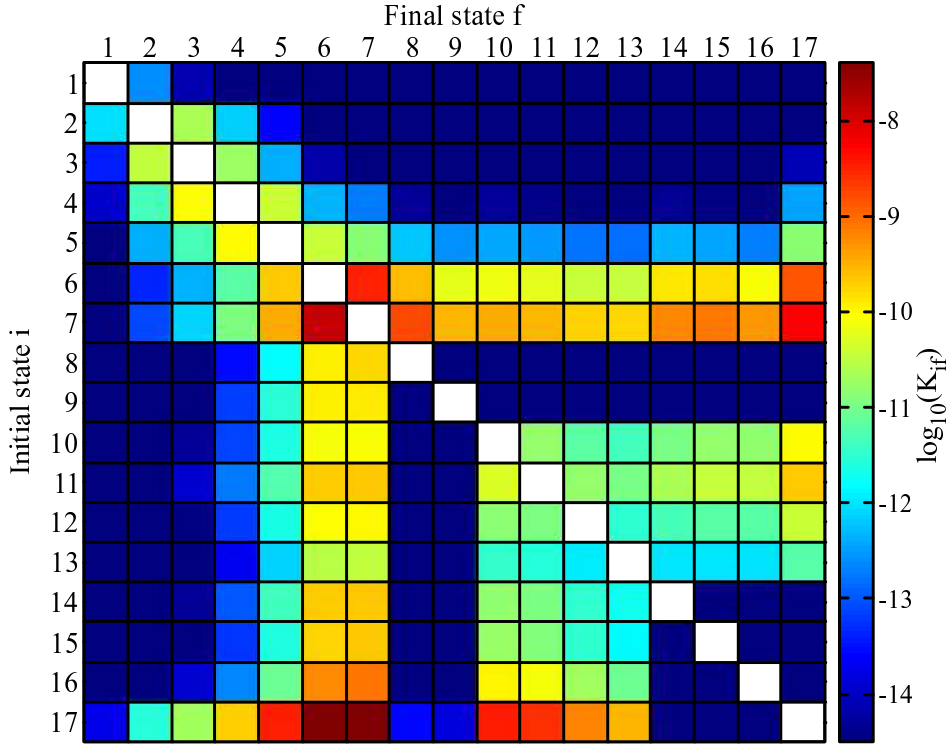


Figure 3. The graphical representation for the inelastic processes rate coefficients in $\text{Sr}(1^3\text{L}) + \text{H}(1s^2\text{S})$ and $\text{Sr}^+(5s^2\text{S}) + \text{H}^-(1s^2\text{1S})$ collisions. The labels for the initial and final states are given in Table 2.

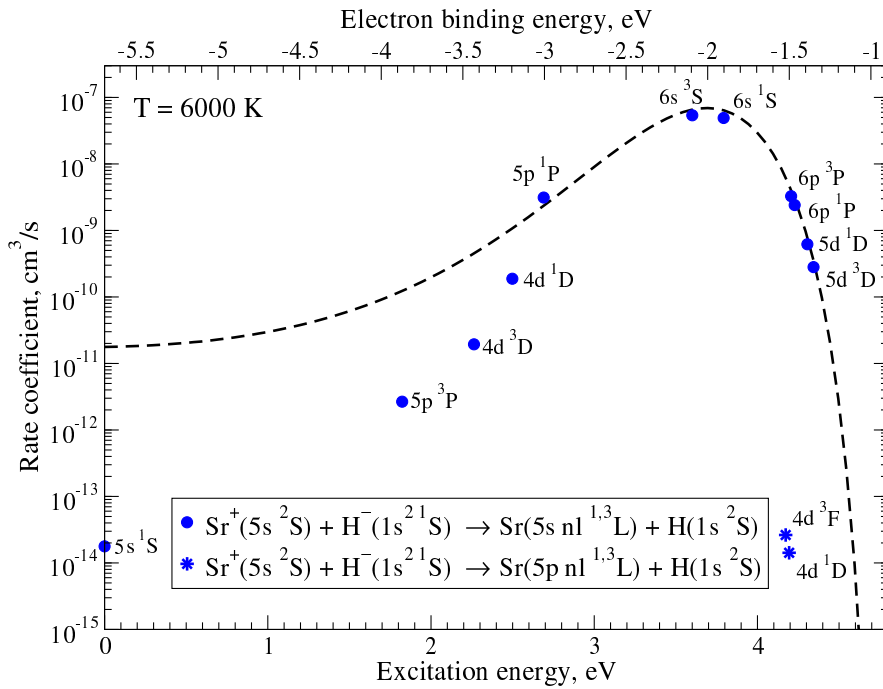


Figure 4. The rate coefficients (in cm^3/s) at $T = 6000\text{ K}$ for the mutual neutralization processes in $\text{Sr}^+(5s^2\text{S}) + \text{H}^-(1s^2\text{1S})$ collisions. Filled circles correspond to the processes due to one electron transitions, stars – to two-electron transitions, dashed line shows the general dependence of the rate coefficient according to the simplified quantum model (Belyaev & Yakovleva 2017a).

3.2 Non-LTE effects for lines of Sr II

In VMP stars, strontium can only be observed in the Sr II 4077 and 4215 Å resonance lines. We used $\log gf(4077 \text{ \AA}) = 0.15$ and $\log gf(4215 \text{ \AA}) = -0.17$, as recommended by the National Institute of Standards and Technology (NIST) database³ (Kramida et al. 2021), and $\log \Gamma_6/N_H = -7.71$ from Barklem & O’Mara (2000). Here, the van der Waals broadening constant Γ_6 corresponds to a temperature of 10 000 K and N_H is the number density of neutral hydrogen.

Figure 5 displays the non-LTE abundance corrections, $\Delta_{\text{NLTE}} = \log \epsilon_{\text{NLTE}} - \log \epsilon_{\text{LTE}}$, for Sr II 4077 Å in the model atmospheres representative of VMP giants ($T_{\text{eff}} = 4500 \text{ K}$) and dwarfs ($T_{\text{eff}} = 5250 \text{ K}$). As found first by Belyakova & Mashonkina (1997), the dominant non-LTE mechanisms for the Sr II resonance lines change, when moving from close-to-solar to the lower metallicity, resulting in a change of negative by positive Δ_{NLTE} . The metallicity, where Δ_{NLTE} changes its sign, depends on T_{eff} , surface gravity $\log g$, and the Sr abundance. This is seen in Fig. 5 for the $T_{\text{eff}} = 5250 \text{ K}$ models. The non-LTE abundance corrections are negative in the models, where Sr II 4077 Å is strong and its core forms in the uppermost atmospheric layers. At these depths, the upper level, $5p^2P_{3/2}^o$, of the resonance transition is underpopulated because of photon losses in the resonance lines, while the ground state keeps its thermodynamic equilibrium population, resulting in decreasing the line source function below the Planck function and an enhanced absorption in the line core. The non-LTE abundance correction for Sr II 4077 Å is positive, if the line forms in deep atmospheric layers, where $5p^2P_{3/2}^o$ is overpopulated by pumping transitions arising from the ground term.

In general, positive Δ_{NLTE} grows toward lower metallicity and lower surface gravity. For given $T_{\text{eff}}/\log g/[\text{Fe}/\text{H}]$, Δ_{NLTE} is larger for the lower Sr abundance ($[\text{Sr}/\text{Fe}]$). For stellar samples, which cover a broad metallicity range and include both dwarfs and giants, neglecting the non-LTE effects for lines of Sr II leads to distorted trends of $[\text{Sr}/\text{Fe}]$ and $[\text{Sr}/\text{Ba}]$ with metallicity and increased scatter of data for stars of close metallicity.

We computed non-LTE abundance corrections for the Sr II 4077 and 4215 Å lines in two grids of the MARCS model atmospheres, which are applicable to VMP dwarfs and giants. For each node ($T_{\text{eff}}/\log g/[\text{Fe}/\text{H}]$) of the grids, the calculations were performed with five $[\text{Sr}/\text{Fe}]$ values. Everywhere, a microturbulence velocity of 1.5 km s^{-1} was adopted. The grids cover the following ranges of atmospheric parameters and Sr abundances.

Grid I: $T_{\text{eff}} = 5000$ to 6500 K , with a step of 250 K ; $\log g = 3.0$ to 5.0 , with a step of 0.5 ; $[\text{Fe}/\text{H}] = -2.0, -2.5, -3.0, \text{ and } -4.0$; $[\text{Sr}/\text{Fe}] = -1.0$ to $+1.0$, with a step of 0.5 .

Grid II: $T_{\text{eff}} = 4000$ to 5000 K , with a step of 250 K ; $\log g = 0.5$ to 2.5 , with a step of 0.5 ; $[\text{Fe}/\text{H}] = -2.0, -2.5, -3.0, \text{ and } -4.0$; $[\text{Sr}/\text{Fe}] = -1.5$ to $+0.5$, with a step of 0.5 .

The entire data set, together with the IDL routine for an interpolation in the grids for given T_{eff} , $\log g$, $[\text{Fe}/\text{H}]$, and observed line equivalent width, are available in machine-readable form⁴.

4 CONCLUSIONS

Rate coefficients for excitation, de-excitation, ion-pair production and neutralization processes in $\text{Sr} + \text{H}$, $\text{Sr}^+ + \text{H}^-$, $\text{Sr}^+ + \text{H}$ and $\text{Sr}^{2+} +$

H^- collisions are calculated using quantum multichannel model approach (Belyaev 2013; Belyaev et al. 2014; Yakovleva et al. 2016). Calculations are performed in the $J - J$ representation for SrH^+ , what allows us to consider 31 scattering channels taking fine structure of Sr^+ into account, and in the $L - S$ representation for SrH considering 17 scattering channels. The inelastic cross sections and inelastic rate coefficients are calculated for 930 partial processes in $\text{Sr} + \text{H}$ and $\text{Sr}^+ + \text{H}^-$ collisions, as well as for 272 partial processes in $\text{Sr}^+ + \text{H}$ and $\text{Sr}^{2+} + \text{H}^-$ collisions; for 1202 partial processes in total.

The Sr II model atom treated by Belyakova & Mashonkina (1997) was updated by using new quantum mechanical rate coefficients for $\text{Sr II} + \text{H I}$ and $\text{Sr II} + \text{H}^-$ collisions. We performed the non-LTE calculations for Sr II with two grids of model atmospheres, which are applicable to VMP dwarfs and giants, and provide the non-LTE abundance corrections for the Sr II 4077 and 4215 Å resonance lines. They are publicly available. The present non-LTE abundance corrections are based on the new atomic data for the inelastic processes in strontium-hydrogen collisions. As the result, the present data are more accurate than the old ones, and hence, the non-LTE modelling is more reliable than the previous ones.

Acknowledgments. SAYa and AKB gratefully acknowledge support from the Ministry for Education and Science (Russian Federation).

5 DATA AVAILABILITY

The calculated rate coefficients are available from the authors.

REFERENCES

- Andrievsky S. M., Spite F., Korotin S. A., François P., Spite M., Bonifacio P., Cayrel R., Hill V., 2011, *A&A*, 530, A105
- Aymar M., Dulieu O., 2012, *Journal of Physics B: Atomic, Molecular and Optical Physics*, 45, 215103
- Barklem P. S., O’Mara B. J., 2000, *MNRAS*, 311, 535
- Barklem P. S., et al., 2005, *A&A*, 439, 129
- Barklem P. S., Belyaev A. K., Guitou M., Feautrier N., Gadéa F. X., Spielfiedel A., 2011, *A&A*, 530, A94
- Bautista M. A., Gull T. R., Ishibashi K., Hartman H., Davidson K., 2002, *MNRAS*, 331, 875
- Belyaev A. K., 2013, *Phys. Rev. A*, 88, 052704
- Belyaev A. K., Lebedev O. V., 2011, *Phys. Rev. A*, 84, 014701
- Belyaev A. K., Yakovleva S. A., 2017a, *A&A*, 606, A147
- Belyaev A. K., Yakovleva S. A., 2017b, *A&A*, 608, A33
- Belyaev A. K., Yakovleva S. A., 2018, *MNRAS*, 478, 3952
- Belyaev A. K., Yakovleva S. A., Barklem P. S., 2014, *A&A*, 572, A103
- Belyaev A. K., Voronov Y., Yakovleva S., 2019, *Physical Review A*, 100, 062710
- Belyakova E. V., Mashonkina L. I., 1997, *Astronomy Reports*, 41, 530
- Bergemann M., Hansen C. J., Bautista M., Ruchti G., 2012, *A&A*, 546, A90
- Bisterzo S., Travaglio C., Gallino R., Wiescher M., Käppeler F., 2014, *ApJ*, 787, 10
- Burbidge E. M., Burbidge G. R., Fowler W. A., Hoyle F., 1957, *Reviews of Modern Physics*, 29, 547
- Butler K., Giddings J., 1985, Newsletter on the analysis of astronomical spectra, No. 9, University of London
- Drawin H. W., 1969, *Zeitschrift für Physik*, 225, 483
- François P., et al., 2007, *A&A*, 476, 935
- Gallagher A. J., Bergemann M., Collet R., Plez B., Leenaerts J., Carlsson M., Yakovleva S. A., Belyaev A. K., 2020, *A&A*, 634, A55
- Gustafsson B., Edvardsson B., Eriksson K., Jorgensen U. G., Nordlund Å., Plez B., 2008, *A&A*, 486, 951

³ <https://physics.nist.gov/PhysRefData/ASD>

⁴ <http://www.inasan.ru/lima/>

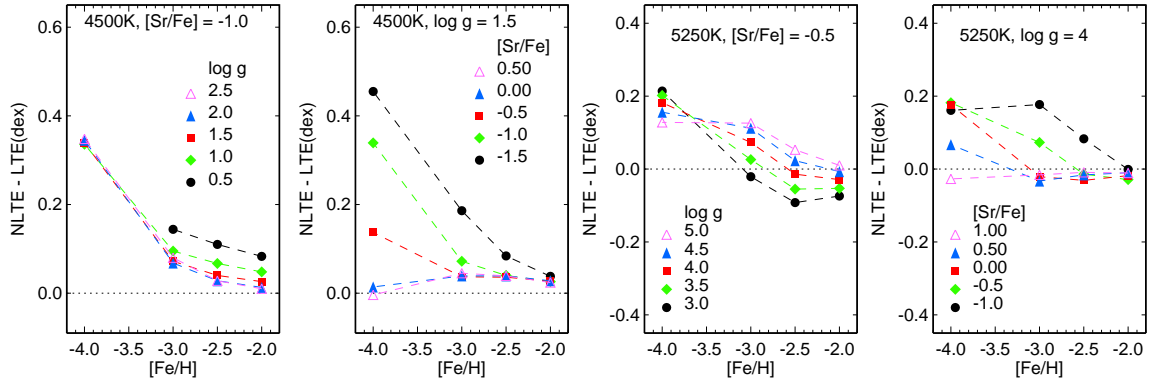


Figure 5. Non-LTE abundance corrections for Sr II 4077 Å in the model atmospheres of giants with common $T_{\text{eff}} = 4500$ K and varied $\log g$ and $[\text{Sr}/\text{Fe}]$ (two left panels) and dwarfs with common $T_{\text{eff}} = 5250$ K and varied $\log g$ and $[\text{Sr}/\text{Fe}]$ (two right panels) as a function of metallicity.

- Honda S., Aoki W., Kajino T., Ando H., Beers T. C., Izumiura H., Sadakane K., Takada-Hidai M., 2004, *ApJ*, 607, 474
- Kramida A., Yu. Ralchenko Reader J., and NIST ASD Team 2021, NIST Atomic Spectra Database (ver. 5.9), [Online]. Available: <https://physics.nist.gov/asd> [2022, January 24]. National Institute of Standards and Technology, Gaithersburg, MD.
- Landau L. D., 1932a, *Phys. Z. Sowietunion*, 1, 88
- Landau L. D., 1932b, *Phys. Z. Sowietunion*, 2, 46
- Lindgård A., Nielson S. E., 1977, *Atomic Data and Nuclear Data Tables*, 19, 533
- Mashonkina L. I., Belyaev A. K., 2019, *Astronomy Letters*, 45, 341
- Mashonkina L., Gehren T., Shi J.-R., Korn A. J., Grupp F., 2011, *A&A*, 528, A87
- Mashonkina L., Jablonka P., Sitnova T., Pakhomov Y., North P., 2017, *A&A*, 608, A89
- McWilliam A., Preston G. W., Sneden C., Searle L., 1995, *Astronomical Journal*, 109, 2757
- Mejrissi L., Habli H., Oujia B., Gadéa F. X., 2018, *International Journal of Quantum Chemistry*, 118, e25680
- Olson R. E., Smith F. T., Bauer E., 1971, *Appl. Opt.*, 10, 1848
- Peach G., 1967, *Memoirs of the Royal Astronomical Society*, 71, 13
- Reader J., Corliss C. H., Wiese W. L., Martin G. A., 1980, *Wavelengths and transition probabilities for atoms and atomic ions: Part 1. Wavelengths, part 2. Transition probabilities.* NIST, USA
- Rizzuti F., Cescutti G., Matteucci F., Chieffi A., Hirschi R., Limongi M., 2019, *MNRAS*, 489, 5244
- Seaton M. J., 1962, in Bates D. R., ed., *Atomic and Molecular Processes*. p. 375
- Sneden C., Cowan J. J., Gallino R., 2008, *ARA&A*, 46, 241
- Steenbock W., Holweger H., 1984, *A&A*, 130, 319
- Yakovleva S. A., Voronov Y. V., Belyaev A. K., 2016, *A&A*, 593, A27
- Zener C., 1932, *Proc. Roy. Soc. A*, 137, 696
- van Regemorter H., 1962, *ApJ*, 136, 906